IMMUNOLOGY

Immunogenic cryptic peptides dominate the antigenic landscape of ovarian cancer

Remya Raja[1]†, Kiran K. Mangalaparthi[2]†, Anil K. Madugundu[2], Erik Jessen[3], Latha Pathangey[1], Paul Magtibay[4], Kristina Butler[4,5], Elizabeth Christie[6,7], Akhilesh Pandey[2,8,9,10], Marion Curtis[1,5,11,12]*

Increased infiltration of CD3$^+$ and CD8$^+$ T cells into ovarian cancer (OC) is linked to better prognosis, but the specific antigens involved are unclear. Recent reports suggest that HLA class I can present peptides from noncoding genomic regions, known as noncanonical or cryptic peptides, but their immunogenicity is underexplored. To address this, we used immunopeptidomic analysis and RNA sequencing on five metastatic OC samples, which identified 311 cryptic peptides (40 to 83 per patient). Despite comprising less than 1% of total peptides, cryptic peptides from noncoding transcripts emerged as the predominant antigen class when compared to the other major classes of known tumor-specific and tumor-associated antigens in OC samples. Notably, nearly 70% of the prioritized cryptic peptides elicited T cell activation, as evidenced by increased 4-1BB and IFN-γ expression in autologous CD8$^+$ T cells. This study reveals noncoding cryptic peptides as an important class of immunogenic antigens in OC.

INTRODUCTION

High-grade serous ovarian cancer (OC) is a lethal gynecological malignancy with a 5-year survival rate of <50% (*1*). Targeted immunotherapies and immune checkpoint inhibitors have proven highly successful in multiple cancer types (*2*). However, patients with OC have limited benefit from these approaches, although several studies have documented the presence of tumor-reactive T cells in OC and shown this to be a positive prognostic factor (*3*, *4*). Presentation of peptides by human leukocyte antigen (HLA) on the cancer cell surface is an essential step in T cell recognition and plays a vital role in the immunosurveillance of cancers (*5*). Therefore, the discovery of tumor-associated or tumor-specific antigens that are recognized by T cells will be crucial for the success of immunotherapeutic approaches in OC.

Mass spectrometry (MS)–based immunopeptidomics is now the only high-throughput approach available to identify and characterize naturally presented HLA class I or class II peptides within the tumor microenvironment (*6*, *7*). Tumor antigen discovery pipelines have mainly focused on the identification of neoantigens derived from patient-specific somatic mutations (*8*, *9*). The presence of neoantigens within tumors robustly correlates with response to immunotherapy (*10*). However, the identification of tumor-reactive neoantigens has been challenging (*11*–*13*), particularly in OC.

Over the past decade, several studies that used genomic-based approaches combined with immunopeptidomics have reported the presence of nonmutated peptides derived from regions of the genome that have been conventionally considered noncoding (*14*–*22*). These noncanonical or cryptic peptides originating from outside the coding exon boundaries are gaining attention as potential tumor-specific antigens owing to their nonmutated status and recurrence among patients with cancer. While there has been substantial interest in discovering cryptic tumor antigens, only one study has reported cryptic peptides in OC, leaving the cryptic antigenic landscape in OC largely unexplored (*16*). Moreover, the immunogenicity of these cryptic peptides is still under investigation, and as a result, their therapeutic potential remains to be fully elucidated.

In this study, we leveraged a proteogenomic approach to identify cryptic HLA class I peptides derived from coding and noncoding regions of the genome from five metastatic ovarian tumors. In contrast to previous studies on gynecologic cancer types, which only identified a maximum of 16 cryptic peptides from noncoding regions in 23 ovarian tumors (*16*) or 21 from four unclassified gynecologic tumors (*22*), our study has discovered 311 cryptic peptides from noncoding regions averaging more than 60 per patient. This study vastly expands the known landscape of cryptic HLA class I antigens in OC. Cryptic peptides were the dominant class of antigens identified. Using patient-matched T cells, we evaluated the antigenicity of 38 cryptic peptides from noncoding transcripts that were selectively up-regulated in tumor tissue compared to adjacent normal tissue. We found that 70% of the candidate cryptic antigens could trigger peptide-specific T cell responses. Our study demonstrates that cryptic peptides from noncoding transcripts constitute a dominant class of immunogenic antigens in OC.

RESULTS

Identification of HLA class I peptides in patients with metastatic OC

To characterize the antigenic landscape of metastatic OC, we performed high-throughput tandem mass spectrometry (MS/MS) analysis to identify class I major histocompatibility complex (MHC)–presented peptides from five patient samples. The clinical characteristics of the patients and HLA information are provided in table S1. In parallel,

[1]Department of Immunology, Mayo Clinic, Phoenix, AZ, USA. [2]Department of Laboratory Medicine and Pathology, Mayo Clinic, Rochester, MN, USA. [3]Division of Computational Biology, Department of Quantitative Health Sciences, Mayo Clinic, Rochester, MN, USA. [4]Division of Gynecology, Mayo Clinic, Phoenix, AZ, USA. [5]College of Medicine and Science, Mayo Clinic, Phoenix, AZ, USA. [6]Peter MacCallum Cancer Centre, Melbourne, Australia. [7]Sir Peter MacCallum Department of Oncology, The University of Melbourne, Parkville, Australia. [8]Mayo Clinic Comprehensive Cancer Center, Mayo Clinic, Rochester, MN, USA. [9]Center for Individualized Medicine, Mayo Clinic, 200 First St SW, Rochester, MN, USA. [10]Manipal Academy of Higher Education, Manipal, Karnataka, India. [11]Department of Cancer Biology, Mayo Clinic, Phoenix, AZ, USA. [12]Mayo Clinic Comprehensive Cancer Center, Mayo Clinic, Phoenix, AZ, USA.
*Corresponding author. Email: curtis.marion@mayo.edu
†These authors contributed equally to this work.

we performed RNA sequencing (RNA-seq) analysis of the tumor specimens, which was used to generate a personalized three-frame translated custom protein database for each patient's tumors. We also called variants from the RNA-seq data, which were then integrated into the respective custom databases. Liquid chromatography (LC)–MS/MS raw data were searched against the personalized proteomic databases to identify various antigen classes, namely the mutated, canonical, or cryptic antigens (Fig. 1A). We first evaluated the number of peptides that were 8 to 12 amino acids long, which is the typical peptide length for HLA class I binders (Fig. 1B). Using the deconvolution algorithm MHCMotifDecon 1.0, we found that, as expected, nearly all class I peptides identified from each sample were predicted to bind HLA alleles that matched with the patient's HLA type (Fig. 1C). In addition, the experimentally derived HLA motifs matched the known sequence motifs for the alleles (Fig. 1D and fig. S1). Overall, these results confirm the robustness of our immunopeptidomic pipeline in identifying peptides that bind class I HLA molecules.

Proteogenomics enables the identification of HLA class I cryptic peptides in OC

The identification of neoantigens is of considerable interest owing to their tumor-specific nature and ability to generate targeted antitumor immune responses. In RNA-seq analysis, we identified a range of 192 to 2056 nonsynonymous mutations among the five patient samples. However, we did not detect any neoantigen-derived peptides in immunopeptidome analysis (fig. S2A).

Given that noncanonical or cryptic peptides constitute a substantial proportion of the HLA class I ligandome (*23*), we next aimed to characterize the cryptic peptidome in OC. On the basis of their genomic origin, we have broadly categorized these peptides into two groups: those derived from regions that contain coding sequences and those originating from noncoding regions of the genome (Fig. 2A). The peptides identified by MS analysis were assigned Gencode biotypes for identifying cryptic peptides and were further stratified by their genomic region. We identified ~6000 to 14,000 peptides per patient, of which cryptic peptides constituted 4.4 to 7.1% of the total (Fig. 2B). A summary of the number of peptides identified per sample is provided in Fig. 2C. The list of cryptic peptides identified by LC-MS/MS is provided in table S2.

Cryptic peptides originating from coding regions such as the 5′ untranslated region (5′UTR) formed the dominant cryptic peptide category, with ~300 to 800 identified per patient, consistent with previous studies (*24*, *25*). However, very few 5′UTR peptides, among the many that have been identified to date, have demonstrable immunogenic potential (*17*, *22*). As a result, we focused on peptides originating from noncoding transcripts as a potential source of antigens. Overall, these peptides accounted for less than 1% of the total immunopeptidome in our dataset, ranging from 40 to 83 per patient (Fig. 2D) for a total of 311 cryptic peptides from 256 unique noncoding RNAs. We then determined whether cryptic peptides displayed any altered physical properties compared to canonical peptides by comparing the hydrophobicity scores of cryptic and canonical peptides against MS retention time. Cryptic peptides displayed no altered distribution in retention time and hydrophobicity when compared with canonical peptides, suggesting no potential bias in their identification relative to canonical peptides (Fig. 2E). Next, we categorized the peptides based on the type of noncoding transcript, and we observed that a large proportion of cryptic peptides originated from pseudogenes, followed by long noncoding RNA (lncRNA) and antisense RNA (Fig. 2F). Overall, these findings are consistent with previously published proteogenomic studies (*26*, *27*).

Cryptic peptides from noncoding transcripts are the major antigen class presented in OC

To determine whether cryptic peptides can be a reliable source for tumor antigens, we compared the number of known tumor-associated antigens (TAAs) and cancer-testis (CT) antigens identified in our dataset to the number of antigens from noncoding transcripts. To assess this, we overlaid the canonical peptidome over the cancer antigen atlas (caAtlas), which is a comprehensive resource generated from publicly available immunopeptidomic datasets from nine cancer types, including OC and 707 benign tissues (*28*). Despite being less than 1% of the immunopeptidome, the cryptic antigens from noncoding transcripts outnumbered all other TAAs or CT antigens detected in our canonical peptidome dataset (Fig. 3A). This observation was consistent in all five samples tested in this study. Up to 8% of the peptides or 20% of the noncoding RNAs detected in our dataset were shared among at least two patients at the peptide and gene levels, respectively (Fig. 3B). Next, we wanted to determine whether these cryptic antigens were expressed across different tumor types. So, we leveraged some of the largest publicly available immunopeptidomic datasets (*22*, *24*) and found that, at the gene level, 45 of 258 cryptic antigens from noncoding transcripts were detected in other cancers, including melanoma (Fig. 3C). The overlap at the peptide level (9 of 311) was reduced compared to the gene level, as expected, considering the diversity of HLA expression across the samples (Fig. 3C). Similarly, we detected an overlap (31 of 256) when the data were compared against the consolidated open reading frames detected from eight ribosomal sequencing (Ribo-seq) datasets (*29*), indicating persistent translation from these regions across tumor types (Fig. 3C). A representative example of a peptide from a noncoding RNA identified in the present study and its corresponding position within the translated Riboseq sequence is shown (Fig. 3D). Rank prediction of the translated protein sequence using NetMHCpan 4.1 shows that the identified peptide is a strong HLA class I binder (Fig. 3E). Together, our results indicate that cryptic antigens from noncoding transcripts could serve as a rich source for immunotherapeutic targets.

In silico prioritization of candidate cryptic peptides for functional validation

Cryptic antigens have been reported in multiple cancers previously (*16*, *17*, *25*). To prioritize peptides for functional validation, we used multiple filtering strategies, as described below, to identify peptides that have a high likelihood of being immunogenic (Fig. 4A). We first used NetMHCpan 4.1 to predict the binding affinity of the cryptic peptides. We found that only a subset of the peptides showed high affinity, defined as <500 nM binding strength, to their cognate HLA (Fig. 4B and fig. S2B). Therefore, to identify peptides with higher likelihood of MHC presentation, predictions were performed using NetMHCpan 4.1-EL, which is trained in eluted ligand data from MS. Peptides were first prioritized using a 4% elution (EL) rank threshold, which was followed by the removal of peptides with gene expression levels less than 0.9 Transcripts per million (TPM) based on our RNA-seq data. Next, we retained peptides from transcripts that were more abundant in the tumor tissue compared to the adjacent normal tissue. We next evaluated whether any of our identified peptides were present in the HLA Ligand Atlas (*30*), an extensive

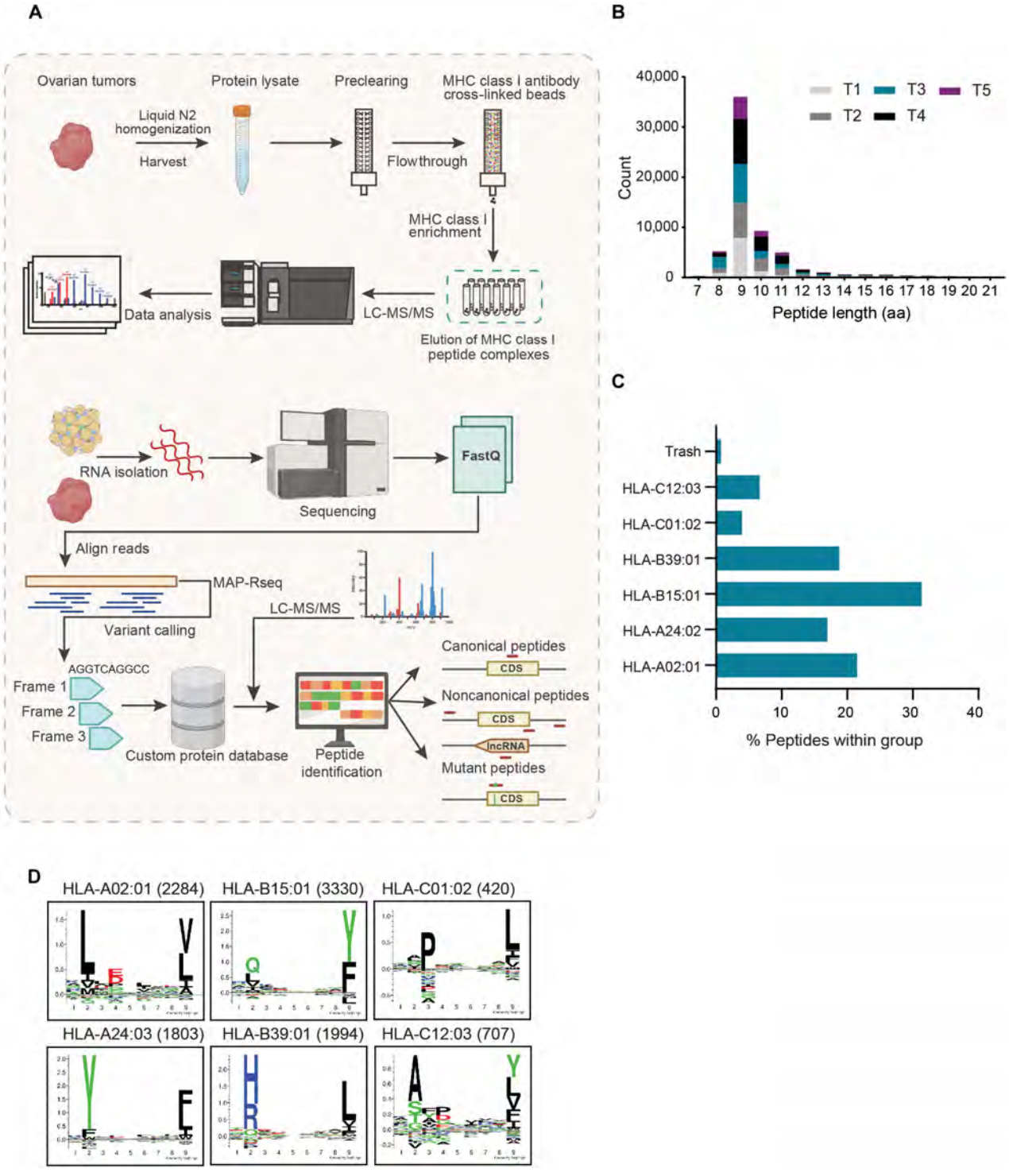

Fig. 1. Identification of HLA class I ligandome in ovarian cancer (OC). (**A**) Schematic overview of the immunopeptidomics approach and proteogenomic pipeline used to identify HLA class I canonical and noncanonical peptides. Class I HLA-bound peptides were purified following immunoprecipitation from tumor lysates and analyzed in the mass spectrometer. The LC-MS/MS data were searched using a 3% false discovery rate (FDR) threshold against a custom three-frame translated database generated from the RNA-seq data. Mayo Analysis Pipeline for RNA sequencing (MAP-RSeq) was employed for variant calling. Created with BioRender.com. (**B**) Length distribution of identified HLA class I peptides. Peptides up to 21 amino acids (aa) in length are shown. (**C**) Peptide deconvolution from sample T1 using NetMHCDecon is depicted. Only 8– to 12–amino acid peptides were used for this analysis. (**D**) Experimentally derived HLA motifs from Sample T1 using NetMHCDecon. The number of peptides predicted to be presented by each HLA is indicated.

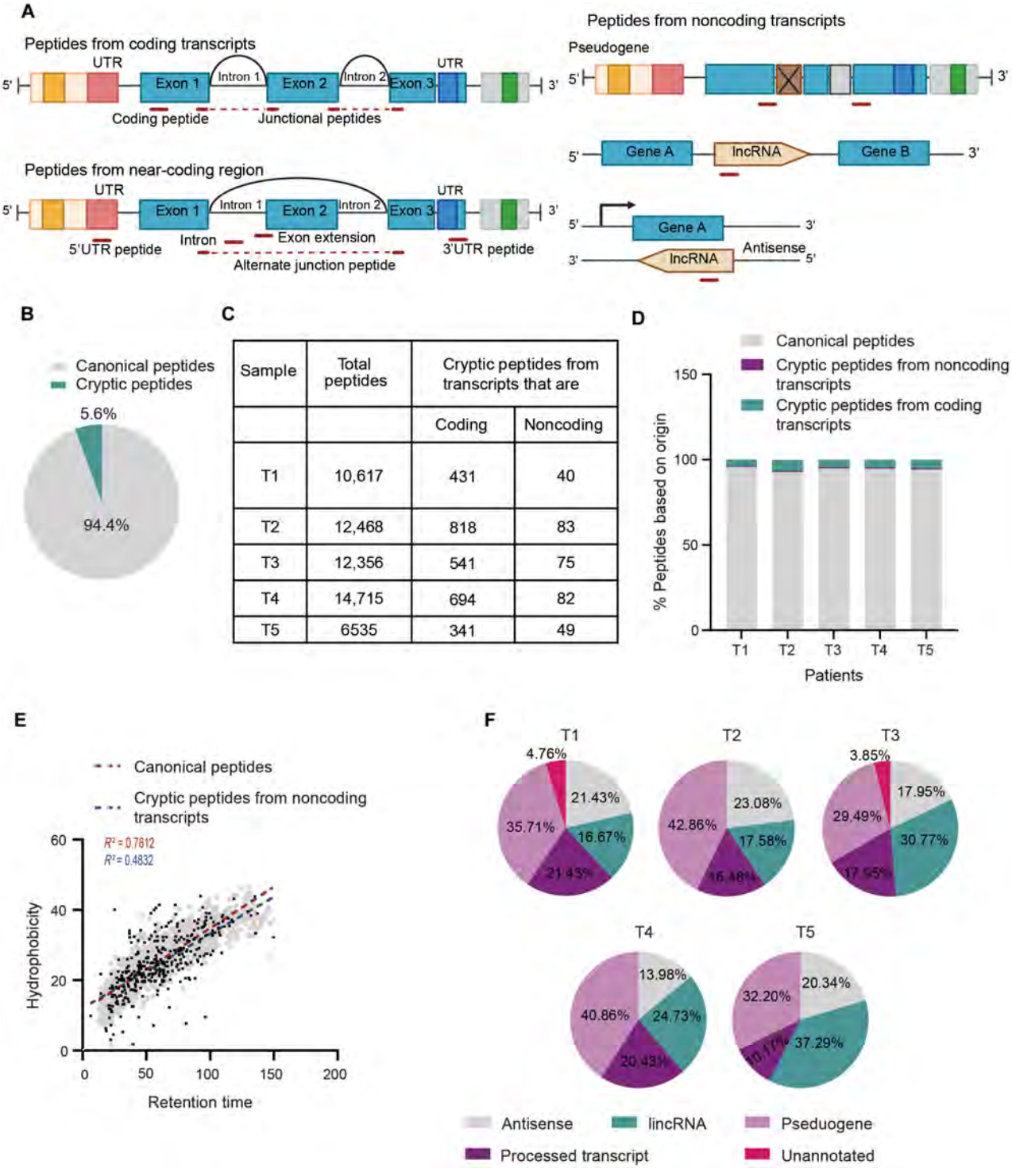

Sample	Total peptides	Cryptic peptides from transcripts that are	
		Coding	Noncoding
T1	10,617	431	40
T2	12,468	818	83
T3	12,356	541	75
T4	14,715	694	82
T5	6535	341	49

Fig. 2. Detection of cryptic HLA class I peptides from noncoding transcripts and their characteristics. (**A**) A schematic illustrating the classification of canonical and cryptic peptides. Cryptic peptides are further categorized on the basis of their site of origin in the genome into peptides from coding and noncoding transcripts. Created with BioRender.com. (**B**) Cryptic peptide composition in the total immunopeptidome is shown. (**C**) The canonical and cryptic peptides identified from each patient sample in this study are enumerated in the table. (**D**) The percentage of peptides contributing to canonical and cryptic categories (coding or noncoding transcript) per patient is shown. (**E**) The retention time of eluted peptides (*x* axis) was plotted against predicted hydrophobicity (*y* axis). Gray dots represent canonical peptides, and cryptic peptides from noncoding transcripts are shown as black dots. The regression line and R^2 are shown, *P* value < 0.0001. (**F**) Peptides were categorized on the basis of the type of noncoding transcripts, and their relative contribution to cryptic ligandome is shown. lncRNA, long noncoding RNA.

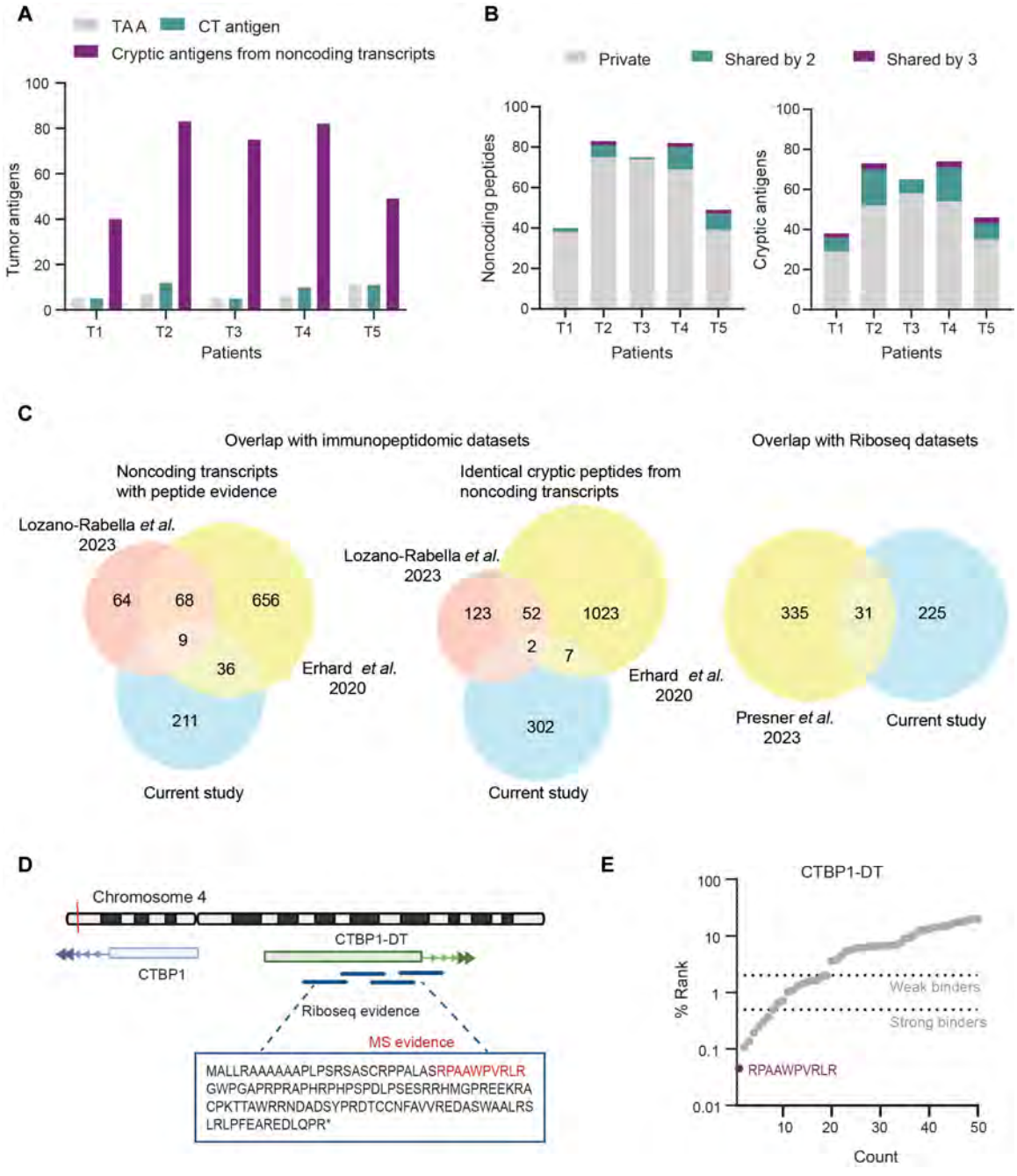

Fig. 3. Cryptic antigens from noncoding transcripts are a reliable source of tumor antigens in OC. (**A**) Total number of peptides identified from each antigen category. Peptides from known OC TAAs and CT antigens were identified using publicly available caAtlas. (**B**) The number of peptides uniquely identified in one patient and those shared among two or three patients is depicted as a bar graph. The tumor antigen representation at the transcript level that is uniquely presented or shared among patients is shown. (**C**) Overlap with publicly available immunopeptidomic (left) and Riboseq (right) datasets are shown. (**D**) A representative example of peptide identified in this dataset with reported Riboseq evidence. (**E**) The rank prediction of all possible peptides binding to HLA-B*07:02 from the translated CTBP1-DT protein. The percentage rank prediction was performed using NetMHCpan4.1. Peptides are considered strong binders (% rank < 0.5) and weak binders (% rank = 0.5 to 2). The peptide derived from CTBP1-DT identified by immunopeptidomics in this study is indicated.

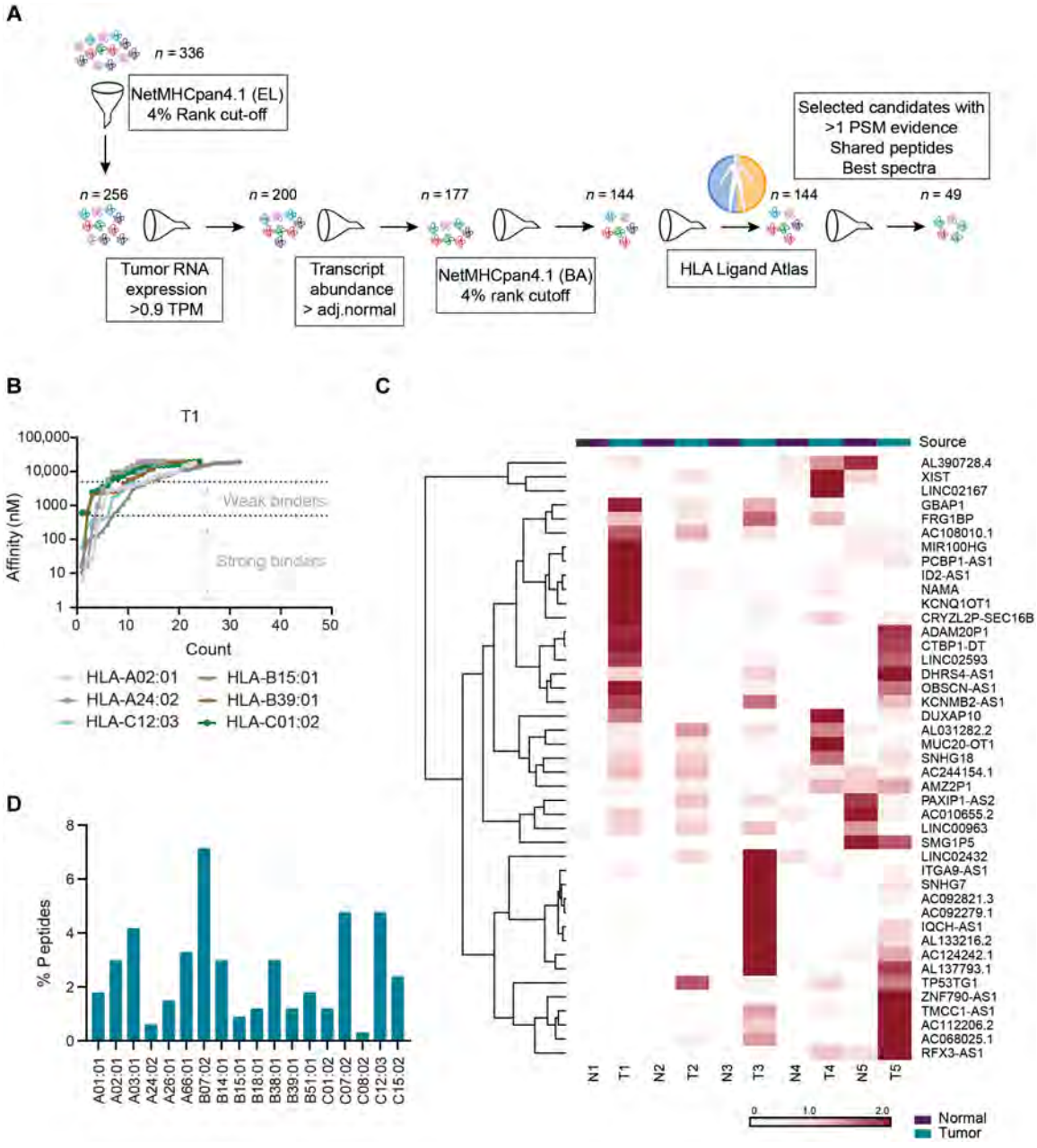

Fig. 4. Identification of candidate noncoding cryptic tumor antigens. (**A**) The prioritization strategy used to derive candidate target antigen is depicted. The peptides were filtered on the basis of % rank EL followed by exclusion of peptides from low-abundance transcripts in the tumor. The possibility of presentation of peptides from normal tissue was ruled out using immunopeptidomic data from healthy and benign tissues (HLA Ligand Atlas). The peptides that had shared presentations or that came from shared noncoding transcripts were prioritized for further studies. (**B**) The binding affinity of peptides predicted to bind to the cognate HLA alleles as per NetMHCpan4.1 for the patient sample T1 is shown. The strong and weak affinity thresholds are indicated using dashed lines at 500 and 5000 nM. (**C**) Heatmap representing the RNA level expression of the 43 prioritized noncoding cryptic antigens in the OC tumor-normal data. For generating the heatmap, gene-level TPM for each of the noncoding RNAs was converted to a *z* score to normalize the dynamic range of expression differences between transcripts. The heatmap was generated using Morpheus (https://software.broadinstitute.org/morpheus). (**D**) Preferential binding of noncoding peptides to their HLA alleles. Peptides that are predicted to be strong binders (% rank < 0.5) by NetMHCpan 4.1 were considered.

database of previously identified HLA class I and II peptides presented across 29 healthy tissues. However, none of the peptides were identified in the HLA Ligand Atlas, suggesting a lack of presentation in normal tissues. Last, we evaluated the spectral quality, shared presentation, and those that were identified with at least two peptide spectrum matches (PSMs) to prioritize peptides. Following these prioritization steps, 9 to 10 peptides were selected from each tumor sample for further analysis. The relative RNA expression of each patient's prioritized antigens in the tumor and adjacent normal tissue is shown (Fig. 4C). A select number of the prioritized cryptic peptides were additionally validated by comparing the experimental peptide spectra with the corresponding synthetic peptide spectra (data file S1). Representative mirror plots showing experimental and synthetic spectra of cryptic peptides are provided (fig. S3).

Previous studies have reported a preferential binding bias for cryptic peptides toward HLA-A*03:01 and HLA-A*11:01 (*14*). To understand whether there was HLA class I binding bias within our noncoding cryptic dataset, we assessed the cryptic peptides within the top 2% rank affinities predicted by NetMHCpan 4.1. Unlike previously published reports, we observed a distinct binding preference toward HLA-B*07:02 rather than HLA-A*03:01 probably due to a smaller sample size representing HLA-A*03:01 (one sample) or HLA-A*11:01, which did not have any representation (Fig. 4D).

Next, we assessed the mRNA expression of the shortlisted noncoding transcripts from this study across 53 normal tissues of the human body using the Genotype-Tissue Expression (GTEx) database to determine whether they are expressed in normal tissues (Fig. 5A). Among the 44 noncoding transcripts, 3 transcripts were not detected in the GTEx data, and the remaining 41 noncoding transcripts were found to have low to moderate expression across peripheral tissues. Among them, many transcripts (11 of 41) were found to have strong expression in tissues with low HLA expression, like the brain, nerve, and testis. Another subset of the transcripts (10 of 41) showed reproductive tissue-restricted expression patterns and showed modest expression in the ovary, vagina, and cervix.

In an effort to understand the temporal dynamics of the cryptic antigen expression in the context of disease progression, we used a previously published RNA-seq dataset from 92 patients with high-grade serous OC (79 primary tumors, 4 primary ascites, 24 recurrent ascites, and 6 relapse tumors) and 7 fallopian tube samples (*31*). Of the 36 prioritized genes, 12 of them were present across multiple stages of disease in the dataset. Among the 12, TMCC1-AS1, DHRS4-AS1, PAXIP1-AS2, and SNHG7 showed significant differences across different stages relative to the primary tumor (Fig. 5B and fig. S4). Overall, we successfully identified 9 to 10 cryptic peptides per patient that were reliably detected by immunopeptidomics, exhibited favorable MHC binding affinity, and had tumor-specific expression.

Cryptic antigen-specific T cell responses are found in patients with OC

We next assessed the potential of the cryptic peptides from noncoding transcripts to induce T cell reactivity following in vitro stimulation of autologous T cells from either ascites or peripheral blood mononuclear cells (PBMCs; Fig. 6A and table S3). After restimulation with peptides, TNF receptor superfamily member 9 (4-1BB), tumor necrosis factor–α (TNFα), and interferon-γ (IFN-γ) expressions were used to measure the antigen-specific CD8 T cell responses by flow cytometry (Fig. 6, B and C, and figs. S5 and S6). Our results showed that approximately 70% of the cryptic peptides could induce an increase in intracellular expression of IFN-γ, and more than 50% of the peptides could also induce TNFα expression in autologous CD8 T cells, demonstrating the potential immunogenicity of these peptides (Fig. 6C). Notably, the peptides that increased IFN-γ expression also had a concomitant increase in 4-1BB expression in CD8 T cells, confirming the antigen-specific activation. In addition, we assessed whether any of the peptides evaluated could trigger CD4 T cell activation. Only a fraction, 8 of 38 peptides induced CD4 T cell activation as measured by increased expression of 4-1BB as well as IFN-γ and TNFα. The corresponding flow plots, along with bar graphs showing the percentage of CD8 T cells expressing IFN-γ, TNFα, and 4-1BB relative to negative peptides, are provided (fig. S7). We plotted the % rank binding affinity (BA) and % rank EL against RNA expression (TPM) to understand the correlation between RNA level expression and the likelihood of presentation on T cell activation. Our results revealed that peptides arising from transcripts that have higher abundance (>4 TPM) showed an increased likelihood of inducing T cell responses (fig. S8, A and B).

Next, we generated HLA-A02:01 MHC class I tetramers for a subset of the HLA-A02:01–restricted peptides that exhibited immune reactivity in samples T1 and T3, to determine whether patients had endogenous T cell clones reactive to cryptic peptides. The proportion of tetramer-positive CD8 cells was evaluated for each peptide individually, and samples showing frequencies more than threefold relative to negative peptide-loaded tetramers were considered positive (Fig. 6D). We detected tetramer positivity in five of six peptides tested, confirming the presence of T cell clones reactive to cryptic peptides in patient samples (Fig. 6D).

Having observed that cryptic peptides could elicit a T cell response in an autologous culture system, we next evaluated whether these noncoding transcripts were associated with protective or spontaneous T cell responses within a large sample of patient tumors. To accomplish this, we first created a score matrix for genes involved in inflammation, T cell invasion, and cytotoxicity. We then used a hierarchical-all-against-all clustering algorithm (HAllA) to correlate the expression of noncoding transcripts in The Cancer Genome Atlas (TCGA) against the T cell activation/infiltration matrix (fig. S8C). We were able to carry out this analysis with 28 of 44 transcripts, which were found to be expressed in the TCGA data. HAllA analysis revealed that noncoding transcripts such as XIST, MUC20-OT1, LINC02432, PAXIP1-AS2, SMG1P5, AC108010.1, and AL390728.4, which generated cytotoxic T lymphocyte responses, showed a strong positive correlation (P value ≤ 0.05) with T cell cytotoxicity and invasion scores, suggesting a potential inflammatory response in the tumor microenvironment. The list of genes involved in inflammation and cytotoxicity in the TCGA data used for HAllA analysis is listed in table S4. Overall, these results suggest that the expression of noncoding transcripts may play a role in shaping the immune microenvironment in OC and could serve as promising therapeutic targets for immunotherapies in OC.

DISCUSSION

Identification of the antigenic landscape of tumors is crucial for the development of effective immunotherapies. The use of standard databases in conventional proteomic approaches precludes the identification of peptides with patient-specific alterations, such as mutations and alternate splice junction peptides, as the peptide

identification relies on the reference human protein database (*14*, *32*). Proteogenomics has been successfully used to obtain a more comprehensive overview of antigenic peptides presented in a sample that can be derived from both coding and noncoding regions of the genome (*33*–*36*). Previous studies have shown that translated products from noncoding regions of the genome are frequently presented by cancer cells and are observed across multiple tumor types accounting to 5 to 10% of the total immunopeptidome (*7*, *15*, *18*, *24*, *25*). In this study, our goal was to comprehensively characterize the tumor antigens generated from noncoding regions of the genome in OC using multiomic approaches and determine their immunogenicity. Most current methods for discovering tumor antigens focus on identifying

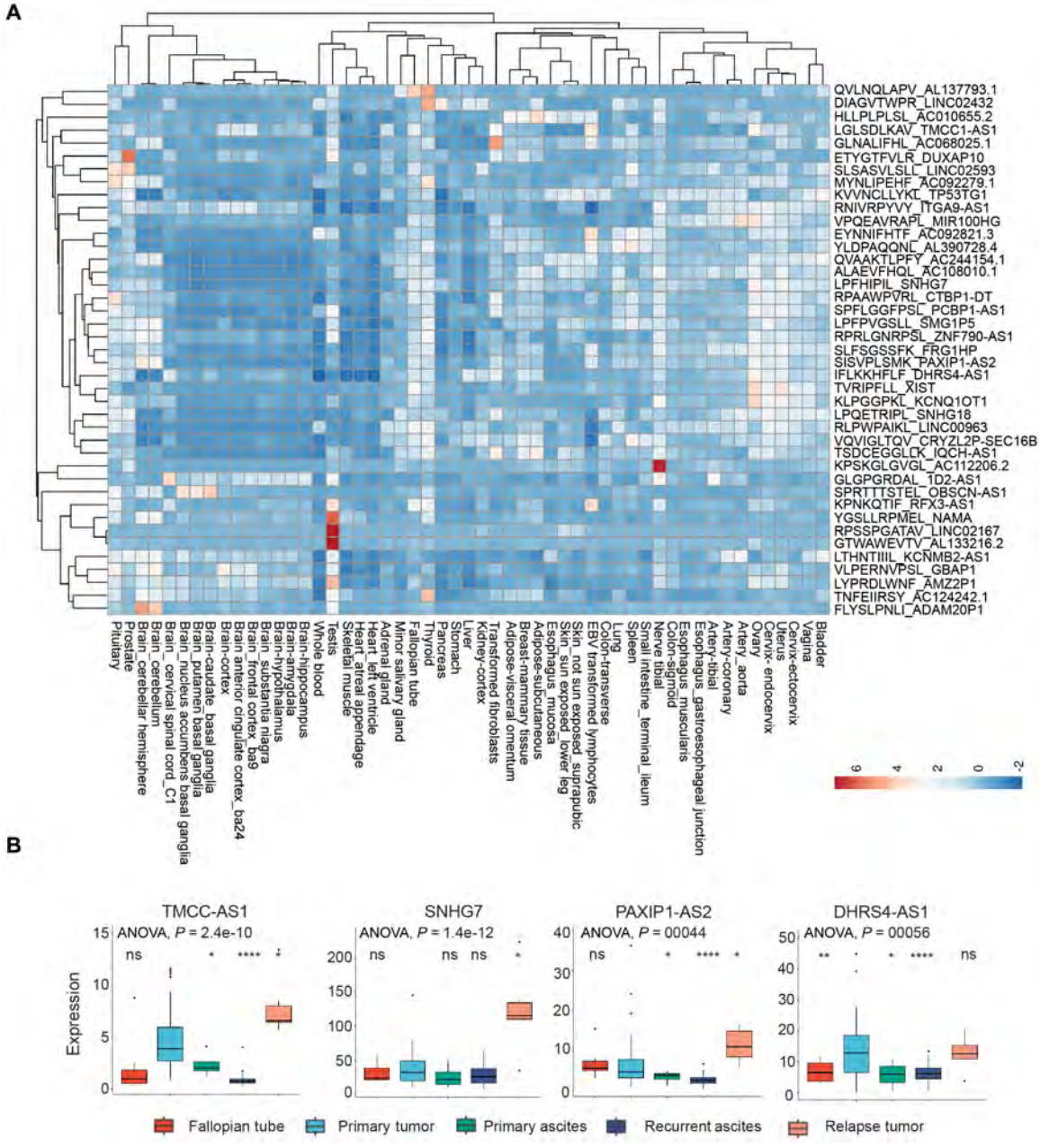

Fig. 5. Noncoding cryptic antigen expression in healthy tissues and various stages of OC progression. (**A**) The expression values of the 41 prioritized noncoding transcripts were compared across 53 normal biological tissues from the GTEx database of normal tissues. Four noncoding transcripts were not detected in the GTEx data. For heatmap generation, the TPM for each noncoding transcript was converted to a *z* score to normalize the dynamic range of expression differences between transcripts. (**B**) RNA expression profiles of four cryptic antigens showing significant variation across the fallopian tube, primary tumor/ascites, and recurrent ascites/relapsed tumors. A publicly available RNA-seq dataset from 113 samples (*31*), including 92 from patients with high-grade serous OC and 7 from normal fallopian tubes, was used to analyze cryptic antigen expression. Twelve antigens were represented in the dataset. Analysis of variance (ANOVA) and *t* test values comparing each sample type to the primary tumor are provided (*$P < 0.05$, **$P < 0.01$, and ****$P < 0.0001$). EBV, Epstein-Barr virus; ns, not significant.

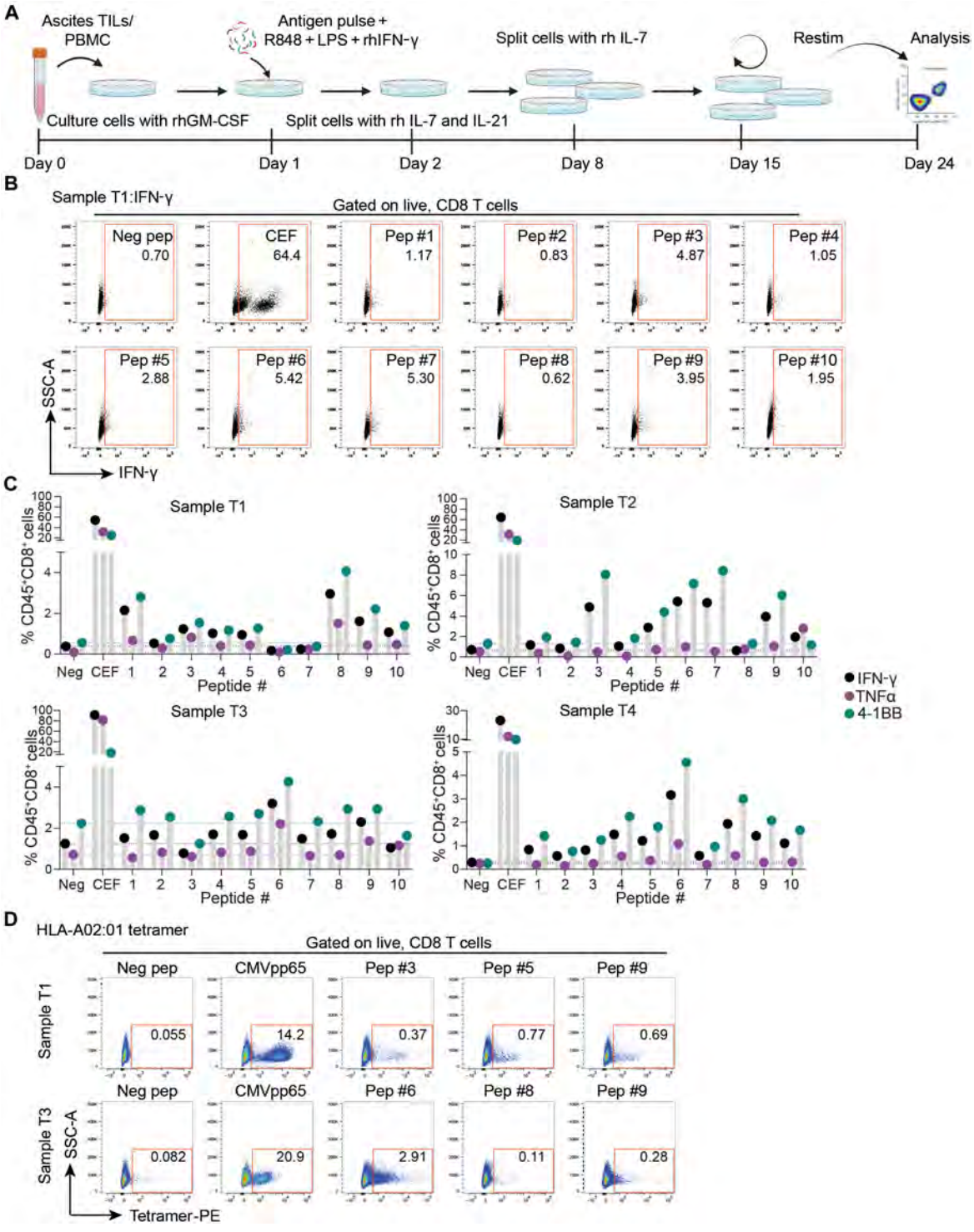

Fig. 6. Noncoding cryptic antigens activate peptide-specific T cell responses in patient-derived T cells. (**A**) A schematic of the workflow used for in vitro stimulation of patient T cells. Patient samples were stimulated with either a negative control peptide (10 μg/ml), the CEF peptide pool (5 μg/ml, positive control), or individual cryptic peptides (10 μg/ml) for 14 days, followed by another round of stimulation on day 15, and cells were expanded for another 8 days. On the day of the assay, the T cells were restimulated with peptide-pulsed autologous tumor cells and analyzed by flow cytometry. CEF is a pool of 32 class I peptides from cytomegalovirus, Epstein-Barr virus, and influenza virus. (**B**) Flow plots of intracellular IFN-γ expression in CD8 T cells from patient sample T2. (**C**) The percentage of CD8 T cells expressing either 4-1BB, TNFα, or IFN-γ following peptide stimulation in four OC samples. The colored dashed lines depict the baseline expression of 4-1BB, TNFα, and IFN-γ in negative peptide (neg pep)–stimulated T cells. (**D**) Frequencies of tetramer-positive CD8 T cell populations in samples T1 and T3 after a 19-day culture. HLA-A02:01–restricted peptides from HIV (gag) and cytomegalovirus (CMV; pp65) were used to generate tetramers that served as negative and positive controls, respectively. rhGM-CSF, recombinant human granulocyte-macrophage colony stimulating factor; LPS, lipopolysaccharide; PE, phycoerythrin.

neoantigens. However, a previous study by Zhao *et al.* (*16*) revealed that neoantigens are rarely found in OC samples, making them unattractive targets in OC. These conclusions are consistent with our findings, where despite the detection of many nonsynonymous mutations (192 to 2056 per patient), we did not identify any corresponding peptides carrying these neoepitopes. The low abundance of mutated class I peptides in advanced OCs could be due to a multitude of factors, including low mutation burden, immunoediting, or strong immune evasive programs like down-regulation of HLA expression (*31*, *37*–*39*). These findings underscore the need to look at alternate sources of target antigens for OC.

Using proteogenomics in this study, we identified approximately 390 to 900 cryptic peptides per patient, averaging ~5% of the total immunopeptidome. Notably, we demonstrated that approximately 70% of the prioritized cryptic peptides from noncoding transcripts induced 4-1BB expression and elicited an IFN-γ response, and around 50% of these also induced TNFα expression in autologous, patient-matched T cells using a scalable patient-derived T cell culture system. To date, only a select few studies have undertaken rigorous testing of cryptic peptides identified by immunopeptidomics to demonstrate the immunogenicity of these antigens conclusively (*14*, *17*, *22*, *39*). In these limited studies, a mere fraction of the antigens was discovered to be immunogenic. For example, Chong *et al.* (*17*), despite testing more than 700 cryptic peptides from melanoma, found only one peptide to be biologically active. The study attributes this lack of recognition by autologous T cells to either prolonged culture of tumor-infiltrating lymphocytes (TILs) or loss of antigen expression in melanoma. In a recent study on OC, Hesnard *et al.* (*40*) found that 13 of 39 (33%) of the tested cryptic antigens were able to trigger a T cell response. This study focused on antigens identified in a previous study of 23 OC tumors that identified 91 cryptic peptides (*16*). However, the research used T cells from HLA-matched healthy donors to assess immunogenicity. This may have led to a suboptimal T cell response, as the cryptic antigen-specific T cells are likely present in limited quantities in peripheral blood from normal donors. Studies have shown that for effective tumor clearance, factors such as peptide-MHC and TCR-peptide-MHC affinities are of critical importance (*41*, *42*). The lack of good prediction algorithms for TCR-peptide affinity has been a major roadblock for developing immunotherapies. Most studies use MHC-peptide prediction algorithms like NetMHC that predict binding affinity between the HLA and peptide but do not take into account the likelihood of endogenous production of the peptide, which leads to high false-positive rates among the predicted epitopes (*43*). Our binding affinity prediction results showed that many of the discovered cryptic peptides exhibited weak predicted affinity to HLA class I, which could be explained by the fact that cryptic peptides are thought to arise from self-antigens that have escaped tolerance (*44*–*46*). Therefore, we relied on NetMHC predictions based on eluted peptides as a key filter criterion for candidate peptides. We also took the RNA-level expression of noncoding transcripts into account as a filtering strategy. Abelin *et al.* (*47*) demonstrated that the level of gene expression is a highly predictive variable for epitope prediction, and RNA-seq serves as a better indicator than MS-based proteomic quantitation. Our data show that peptides derived from abundant transcripts were more likely to induce an immune response, which is not unexpected as increased expression improves the likelihood of being presented by the HLA.

The specificity of expression of cryptic peptides in tumor tissues is vital for developing effective immunotherapies. In this study, we found that while a subset of the noncoding RNAs was not detected in healthy RNA-seq data from GTEx, quite a few had low to moderate RNA expression across healthy tissues. It is important to note that the transcript abundance alone is not predictive of the noncanonical translation of these peptides. Lozano-Rabello *et al.* (*22*) have reported that the lack of presentation in healthy tissues indicates the tumor-specific nature of these cryptic peptides. Our study suggests that our in silico prioritization pipeline, which incorporated many critical factors, including HLA binding affinity, tumor expression, and expression in normal tissues, was highly successful in identifying immunogenic antigens in a patient-specific manner.

These findings may also have broader implications for other cancer types with low mutational burden, where neoantigens are rare (*48*). There is a clear need for larger-scale studies to identify the abundance of cryptic antigen expression across different tumor types and also understand how cryptic antigen burden may correlate with clinical responses to immunotherapy. Such studies could pave the way for the future development of immunotherapies targeting cryptic antigens in additional tumor types. Moreover, understanding how cryptic antigens are processed and presented could provide innovative strategies to enhance immune recognition. In the long term, these efforts could broaden the reach of immunotherapy, making it viable for a wider range of cancers that now lack effective treatment options.

Recent trials of neoantigen vaccines have shown promising results, making personalized cryptic antigen-based vaccines an appealing treatment strategy. For example, NEO-PV-01, a long peptide cancer vaccine that included 20 neoantigens, was tested in combination with Nivolumab and was shown to induce the cytotoxic neoantigen-specific T cells in patients with non–small cell lung cancer, melanoma, and bladder cancer (*49*). The demonstrated efficacy of severe acute respiratory syndrome coronavirus 2 mRNA vaccines has provided substantial momentum in the field, leading to several clinical trials evaluating anticancer mRNA vaccines in combination with immune checkpoint inhibitors and other immunotherapies. A previous study by Sahin *et al.* (*50*) demonstrated the first-in-human application of an mRNA-based neoantigen vaccine that could effectively inhibit melanoma recurrence, leading to sustained progression-free survival. Recently, a phase 2b trial that tested a multiantigen, personalized cancer vaccine delivered with mRNA was reported to reduce the recurrence of melanoma when combined with pembrolizumab (*51*). In this context, our study suggests that developing personalized antitumor vaccines targeting cryptic antigens in OC could be an effective therapeutic approach.

One limitation of our study is that we have mainly concentrated on peptides derived from long noncoding RNA and pseudogenes, potentially overlooking other types of antigens that were not well represented in our dataset, like peptides from retroviral elements (*52*, *53*). Detection of human endogenous retrovirus (HERV)-derived peptides would require bioinformatic pipelines to quantify HERV expression and merge this information with custom protein databases (*17*, *54*). Therefore, this class of antigens may be underrepresented in our dataset, and a more complex bioinformatic pipeline could be developed to understand their contribution to the antigen landscape of OC in the future. Another limitation of our study is the small sample size, which may affect the characteristics

of the cryptic peptides that we identified. Also, all the patients included in our study had advanced metastatic disease. In future studies, it will be important to understand how the stage and grade of OC tumors may influence the cryptic antigen landscape.

Evaluating autologous T cell responses to cryptic antigens using preclinical mouse models would provide important insights into the therapeutic potential of these antigens. However, assessing autologous human T cell responses in mouse models presents several technical challenges and limitations, including HLA incompatibility, graft-versus-host disease, and genomic differences between human and mouse diseases. Despite these limitations, such studies in the future could offer valuable insights into the role of cryptic antigens in shaping antitumor immunity.

Our research shows that cryptic peptides are the primary class of tumor antigens in OC. These peptides are immunogenic and may play a role in the observed clinical immune responses against OC. Overall, they represent a promising source of antigens for the potential future development of targeted immunotherapies.

MATERIALS AND METHODS

Patient samples

All samples were collected at Mayo Clinic Arizona after obtaining informed consent from women diagnosed with advanced-stage OC. The Institutional Review Board (IRB) of the Mayo Clinic approved the study protocol and the consent form (application #18-010082). Deidentified patient characteristics are provided in table S1. The tumor and the corresponding adjacent normal tissue were obtained after primary debulking on the procedure's day. Ascites samples were collected from patients who underwent ascites drainage. The tumor and adjacent normal tissue were snap-frozen for RNA-seq. A part of frozen tumors or ascites cell pellet (sample T3) following red blood cell (RBC) clearance was used for immunopeptidome analysis. Fresh tissues were used to isolate stromal vascular fraction (SVF) and tumor digests for T cell stimulation studies.

RNA sequencing

RNA-seq was performed by an external service provider (Genewiz, NJ). Briefly, RNA was isolated from cryopreserved tissue using the RNeasy Mini Kit (QIAGEN). One microgram of isolated RNA was used to prepare single index libraries using a TruSeq Stranded total RNA kit (Illumina) following ribosomal RNA (rRNA) depletion using a Riboseq rRNA depletion kit. The final library sizes were assessed using the Agilent TapeStation, and concentration was determined by Qubit assay. Paired-end sequencing was performed in a HiSeq platform with a read length of 150 bp and a target read depth of at least 50 million reads.

HLA typing

HLA typing was performed from the genomic DNA isolated from a patient PBMC by next-generation sequencing (Creative Biolabs, New York, USA).

Enrichment of MHC-bound peptides from primary human OC samples

Enrichment of MHC class I–bound peptides was performed as described before (*55*, *56*). Five milligrams of pan-specific MHC class I antibody (W6/32 clone) and 1 ml of Protein A–Sepharose 4B beads (Invitrogen) were used to prepare antibody cross-linked columns. Cross-linking was facilitated by incubating the columns with 20 mM dimethyl pimelimidate linker for 45 min. The cross-linking reaction was quenched with 5 mM ethanolamine (pH 8.0). Columns were then washed with phosphate buffer saline and stored in phosphate-buffered saline (PBS)/0.02% sodium azide at 4°C. Before the enrichment, columns were washed with 1 ml of 0.1 N acetic acid followed by 10 ml of 100 mM tris HCl (pH 8.0). Ovarian tumor tissues were homogenized using liquid nitrogen and resuspended in 6 ml of lysis buffer (0.25% sodium deoxycholate, 0.2 mM indole-3-acetic acid, 1 mM EDTA, 1 mM phenylmethylsulfonyl fluoride, 1% octyl-β-glucopyranoside, and 1:200 protease inhibitor cocktail) and incubated for 1 hour at 4°C. Ascites fluid is centrifuged at 14,000 rpm to pellet down the cells. The cell pellet was resuspended in lysis buffer and processed as performed for tumor tissues. Protein lysates were centrifuged at 14,000 rpm for 1 hour and loaded on a column with just Protein A–Sepharose 4B beads for preclearing. The flowthrough was then loaded onto the antibody cross-linked columns and incubated for 2 hours with rotation at 4°C. The column containing the beads with enriched MHC-peptide complexes was washed with 10 ml of 150 mM NaCl in 20 mM tris HCl (pH 8.0), 400 mM NaCl in 20 mM tris HCl (pH 8.0), followed by 150 mM NaCl in 20 mM tris HCl (pH 8.0) and 20 mM tris HCl (pH 8.0). MHC-bound peptide complexes were eluted using 1% trifluoroacetic acid, and peptides were purified on C_{18} stage tips and concentrated using SpeedVac.

LC-MS/MS analysis of MHC-bound peptides

Peptides were resuspended in 6 μl of 2% acetonitrile/0.1% formic acid and analyzed on a Orbitrap Eclipse Tribrid mass spectrometer connected to UltiMate RSLC3000 nanoLC system (Thermo Fisher Scientific, San Jose, CA). NanoLC was operated in a two-column mode which includes a trap column (PepMap C_{18} 2 cm by 100 μm, 100 Å) for the initial trapping of peptides and an analytical column (EasySpray 50 cm by 75 μm, C_{18} 1.9 μm, 100 Å; Thermo Fisher Scientific, San Jose, CA) for separation of peptides. Before sample loading, both columns were equilibrated using 0.1% formic acid (solvent A) for 10 min. Elution of peptides was done using a gradient of 7 to 28% solvent B (acetonitrile/0.1% formic acid) for 115 min and then to 40% for 10 min. Last, the columns were washed with 80% solvent B for 5 min. As the peptides were being eluted, the mass spectrometer was operated in a data-dependent mode in which the precursor ions were recorded in a survey MS scan followed by MS/MS analysis for a cycle time of 2 s. MS scan was recorded at 60 K resolution [at 200 mass/charge ratio (m/z)], 4×10^{-5} automatic gain control (AGC) target, and 50-ms injection time for a mass range of 350 to 1400 m/z in Orbitrap analyzer. MS/MS analysis was performed separately for charge state 2 to 4 (scan priority 1) and charge state 1 within the mass range of 700 to 1400 m/z (scan priority 2). Highly abundant precursor ions were isolated using 1.4 m/z isolation width in quadrupole, subjected to higher-energy collisional dissociation (HCD) fragmentation at 28% (scan priority 1) and 32% (scan priority 2). Fragment ions were recorded in an Orbitrap analyzer at 30,000 resolution, 1×10^{-5} AGC target, and 100 ms injection time. Monoisotopic precursor selection and a minimum intensity threshold of 20,000 counts were applied before precursor ion selection for MS/MS analysis. Precursors once fragmented were prevented from repeated analysis by using a dynamic exclusion filter for an exclusion duration of

40 s. Internal mass calibration was performed using a lock mass of 445.12002 *m/z*.

Custom database generation and identification of MHC-bound cryptic peptides

Fastq data from RNA-seq analysis of tumor and normal samples were checked for quality using FastQC software. Adapter sequence and low-quality bases in reads were trimmed using the Cutadapt tool (http://dx.doi.org/10.14806/ej.17.1.200). Quality processed reads were then aligned with human reference (GRCh38) and GENCODE v29 annotations using STAR aligner in two-pass mode by using a database of exon-exon junctions detected across samples in the first step to generate final alignment BAM files (*57*). STAR-aligned BAM files were further processed by marking duplicates, split CIGAR string, base recalibration, variant calling, and filtering using genomic analysis toolkit (GATK). Detection of somatic mutations in matched tumor-normal samples was carried out using VarScan2 software. Identified germ-line and somatic variants were annotated using SnpEff. Predicted nonsynonymous changes are then incorporated into reference protein sequences to generate a custom variant peptide database of single nucleotide polymorphisms (SNPs) using an in-house script written in Python programming language. Reference-based transcript assembly and annotations against GENCODE features were carried out using StringTie (*58*). Identified transcripts were translated into peptide sequences in forward three frames.

MS raw data files were analyzed for peptide identification using both the Sequest search engine in Proteome Discoverer (version 2.5) and MSFragger in FragPipe v15 (*59*, *60*). Database searching was performed by in silico digestion of sample-specific personalized protein databases with no enzyme specificity and peptide length of 7 to 25 amino acids. Precursor ion tolerance of 10 parts per million (ppm), fragment ion tolerance of 0.05 Da, and dynamic modifications such as oxidation (M), cysteinylation (C), and deamidation (N and Q) were used in Sequest. In MSFragger, precursor and fragment ion tolerance of 20 ppm, oxidation (M), acetylation at protein N terminus, and cysteinylation (C) were used as dynamic modifications. The false discovery rate (FDR) was controlled by Percolator, and identifications were filtered to 3% at the PSM level for both search engines (*14*, *61*). Furthermore, peptides mapping to "protein_coding," "IG_C_gene," and "IG_V_gene" or HLA transcript biotypes were excluded to derive the cryptic peptides. The cryptic peptides were further stratified on the basis of the genomic origins into near-coding and noncoding. MHC-bound peptide identifications from the noncanonical regions were selected for functional validation and were verified by manually checking MS/MS spectra.

Motif deconvolution of immunopeptidomic data

The multiallelic immunopeptidomic data were deconvoluted using the benchmarked MHCMotifDecon-1.0 (https://services.healthtech.dtu.dk/service.php?MHCMotifDecon-1.0). The method uses a supervised approach wherein the peptides are assigned to the most likely class I HLA type based on the MHC binding predictions from NetMHCpan-4.1, and the potential contaminants are placed in a trash bin (*62*). We compared the resulting motifs to the known and predicted motifs of the HLA class I alleles using the MHC motif viewer (*63*).

Class I affinity predictions

The NetMHCpan 4.1 EL prediction method was used to identify peptides that have a higher likelihood of being naturally processed and presented. In parallel, the binding affinity of HLA class I peptides was predicted using the NetMHCpan-4.1BA (http://tools.iedb.org/mhci/) based on the patient-specific allotypes as determined by HLA typing. For class I predictions, 8- to 12-mer peptides were used as input. Peptides with a predicted binding rank of ≤0.5 or 500 nM were considered high-affinity binders (*64*).

Peptide hydrophobicity analysis

The hydrophobicity values for noncoding and canonical peptides were calculated using the peptide analysis tool from Thermo Fisher Scientific (https://thermofisher.com/us/en/home/life-science/protein-biology/peptides-proteins/custom-peptide-synthesis-services/peptide-analyzing-tool.html), and the values were plotted against the corresponding MS retention time in GraphPad Prism (v10.1.1).

Normal tissue expression of candidate noncoding transcripts

The expression values of the 41 noncoding transcripts were compared across different biological tissues from the GTEx database of normal tissues. For plotting, each noncoding transcript was converted to a *z* score to normalize the dynamic range of expression differences between transcripts. The data used for the analyses described in this manuscript were obtained from UCSC from the BED file (/gbdb/hg19/gtex/gtexTranscExpr.bb).

HAllA correlations of noncoding transcripts to inflammation and cytotoxicity

Correlation of noncoding transcript expression to inflammation and cytotoxicity lists was performed using the HAllA (*65*). Associations with an adjusted *P* value less than 0.05 were considered significant. In addition, the inflammation and cytotoxicity were summarized per TCGA sample as an average expression *z* score value of all genes in each gene list. The *z* score was calculated on the basis of TCGA average expression and SD for each gene across all samples. The summarized metric was used in HAllA to associate noncoding transcript expression with summarized inflammation and cytotoxicity metrics.

Tumor dissociation for TIL isolation

Tissues were minced into small pieces and transferred to magnetic-activated cell sorting (MACS) C tubes containing tissue dissociation mix [collagenase II (2 mg/ml) and deoxyribonuclease I (30 μg/ml)]. Tissue digestion was carried out for 1 hour using the OctoMACS system (Milteny Biotech). Single-cell suspensions were obtained after filtration with 70-μm filters. Erythrocytes were lysed using RBC lysis buffer (Tonbo Biosciences, #TNB-4300). After two washes with PBS, the cells were cryopreserved till further use.

Isolation of TILs from SVF and ascites

Omental tissue was cut into small (3 to 5 mm) pieces and transferred to 250-ml Erlenmeyer flasks. Tissue digestion was performed using collagenase type I (17-100-017, Thermo Fisher Scientific) in a rotating shaker incubator at 37°C at 180 rpm for 1 hour. The tissue digest was filtered through a mesh-lined funnel and collected. The cell suspension was centrifuged to remove the top adipocyte layer. The RBCs in the pellet (SVF) were lysed using 1× RBC lysis solution. Cells after two washes with PBS were cryopreserved until further use. Ascitic fluid was subjected to low-speed centrifugation (300*g*, 5 min). RBCs were lysed, and the cells were washed thoroughly with 1× PBS. The washed cells were cryopreserved and later used for TIL expansion.

In vitro T cell expansion and antigen-specific activation

In vitro, omentum-derived TILs or PBMCs from patients with OC were peptide-stimulated and expanded as described previously with minor modifications (*66*). Omentum-derived cells thawed on day 0 and were resuspended in AIM-V media (Gibco, #0870112-DK) with 0.5% human AB serum (Gemini Bioproducts, #100-512) and granulocyte-macrophage colony-stimulating factor (80 ng/ml; Tonbo Biosciences, #21-8339-U020). On day 1, the cells were stimulated with individual peptides (10 μg/ml). At 4 hours after antigen pulsing, Resiquimod (R848, 6 μg/ml; STEMCELL Technologies, #73782) was given, followed by lipopolysaccharide (10 ng/ml, InvivoGen, #TLRL-3PELPS) and recombinant human (rh) IFN-γ (500 IU/ml; PeproTech, #300-02) after 30 min. On day 2, the cells were collected from wells and resuspended in AIM-V media with 2% AB serum with rh interleukin-21 (IL-21; 6 ng/ml; BioLegend, #571202) and IL-7 (50 ng/ml; BioLegend, #581904) (*67*). The cells were split on day 8, and the media was replenished. The cells were expanded with intermittent splits, and media was changed every 4 days. On day 15, cells were given a second antigenic pulse, followed by expansion till day 21. Between days 21 and 24, the cells were collected for downstream assays.

Flow cytometry

For IFN-γ intracellular staining, the cells were restimulated with peptide-pulsed autologous tumor cells and treated with 1:1000 Golgi plug (BD Biosciences, #555029) and 1:1500 Monensin (Tonbo Biosciences, #TNB-4505-L001). As positive control, pool of 32 class I peptides from cytomegalovirus, Epstein-Barr virus, and influenza virus (CEF; STEMCELL Technologies, #100-0675) was used. The cells were stained with anti-human CD45 (Tonbo Biosciences, #25-0459-T100), CD8 (BioLegend, #344724), and CD4 (Tonbo Biosciences, #65-0048-T100) and processed to measure intracellular IFN-γ (BioLegend, #502509), TNFα (BioLegend, #502932), and cell surface 4-1BB (Cytek Biosciences, #SKU 63-1379-42) after 16 hours of peptide stimulation for flow cytometry. Peptide-MHC class I tetramers were generated by peptide exchange using a QuickSwitch Quant HLA A02:01 Tetramer kit-Phycoerythrin (PE) (MBL International Corporation, #TB-7300-K1) as per the manufacturer's instructions. Peptide pulsed T cells were treated with 50 nM dasatinib for 30 min at 37°C before tetramer staining, followed by surface staining with anti-human CD45 and CD8 as described previously (*68*). Tetramers containing an HLA-A02–restricted peptide from HIV (gag: SLYNTVATL) was used as a negative control, and a peptide from cytomegalovirus (pp65: NLVPMVATV) was used as a positive control.

Statistics and visualization of data

All graphs were prepared using GraphPad Prism (GraphPad, La Jolla, CA). Differences were considered significant if $P < 0.05$. Hierarchical all-against-all clustering was performed using HAllA, and significant associations were determined by FDR < 0.05 (*65*). Heatmaps were generated using the ggplot2 R package (Rv4.3.2) or Morpheus (https://software.broadinstitute.org/morpheus). One-way analysis of variance (ANOVA) combined with Student's *t* test was performed to compare the RNA level expression of noncoding transcripts across various stages of ovarian tumor progression.

Ethics approval and consent to participate

Ascites/tumor/blood was collected from patients with OC undergoing primary debulking surgery by a gynecologic oncologist at the Mayo Clinic Hospital, Arizona. Informed consent was obtained before surgery, and the study was approved by the IRB of the Mayo Clinic (application #18-010082).

Supplementary Materials

The PDF file includes:

Figs. S1 to S8
Data file S1
Legends for tables S1 to S4

Other Supplementary Material for this manuscript includes the following:

Tables S1 to S4

REFERENCES AND NOTES

1. C. Allemani, T. Matsuda, V. Di Carlo, R. Harewood, M. Matz, M. Niksic, A. Bonaventure, M. Valkov, C. J. Johnson, J. Esteve, O. J. Ogunbiyi, E. S. G. Azevedo, W. Q. Chen, S. Eser, G. Engholm, C. A. Stiller, A. Monnereau, R. R. Woods, O. Visser, G. H. Lim, J. Aitken, H. K. Weir, M. P. Coleman, CONCORD Working Group, Global surveillance of trends in cancer survival 2000-14 (CONCORD-3): Analysis of individual records for 37 513 025 patients diagnosed with one of 18 cancers from 322 population-based registries in 71 countries. *Lancet* **391**, 1023–1075 (2018).
2. P. Sharma, J. P. Allison, Immune checkpoint targeting in cancer therapy: Toward combination strategies with curative potential. *Cell* **161**, 205–214 (2015).
3. L. Zhang, J. R. Conejo-Garcia, D. Katsaros, P. A. Gimotty, M. Massobrio, G. Regnani, A. Makrigiannakis, H. Gray, K. Schlienger, M. N. Liebman, S. C. Rubin, G. Coukos, Intratumoral T cells, recurrence, and survival in epithelial ovarian cancer. *N. Engl. J. Med.* **348**, 203–213 (2003).
4. E. Sato, S. H. Olson, J. Ahn, B. Bundy, H. Nishikawa, F. Qian, A. A. Jungbluth, D. Frosina, S. Gnjatic, C. Ambrosone, J. Kepner, T. Odunsi, G. Ritter, S. Lele, Y. T. Chen, H. Ohtani, L. J. Old, K. Odunsi, Intraepithelial $CD8^+$ tumor-infiltrating lymphocytes and a high $CD8^+$/regulatory T cell ratio are associated with favorable prognosis in ovarian cancer. *Proc. Natl. Acad. Sci. U.S.A.* **102**, 18538–18543 (2005).
5. M. Y. Lee, J. W. Jeon, C. Sievers, C. T. Allen, Antigen processing and presentation in cancer immunotherapy. *J. Immunother. Cancer* **8**, e001111 (2020).
6. C. Chong, G. Coukos, M. Bassani-Sternberg, Identification of tumor antigens with immunopeptidomics. *Nat. Biotechnol.* **40**, 175–188 (2022).
7. M. Bassani-Sternberg, E. Braunlein, R. Klar, T. Engleitner, P. Sinitcyn, S. Audehm, M. Straub, J. Weber, J. Slotta-Huspenina, K. Specht, M. E. Martignoni, A. Werner, R. Hein, D. H. Busch, C. Peschel, R. Rad, J. Cox, M. Mann, A. M. Krackhardt, Direct identification of clinically relevant neoepitopes presented on native human melanoma tissue by mass spectrometry. *Nat. Commun.* **7**, 13404 (2016).
8. T. N. Schumacher, R. D. Schreiber, Neoantigens in cancer immunotherapy. *Science* **348**, 69–74 (2015).
9. Y. C. Lu, P. F. Robbins, Cancer immunotherapy targeting neoantigens. *Semin. Immunol.* **28**, 22–27 (2016).
10. N. McGranahan, A. J. Furness, R. Rosenthal, S. Ramskov, R. Lyngaa, S. K. Saini, M. Jamal-Hanjani, G. A. Wilson, N. J. Birkbak, C. T. Hiley, T. B. Watkins, S. Shafi, N. Murugaesu, R. Mitter, A. U. Akarca, J. Linares, T. Marafioti, J. Y. Henry, E. M. Van Allen, D. Miao, B. Schilling, D. Schadendorf, L. A. Garraway, V. Makarov, N. A. Rizvi, A. Snyder, M. D. Hellmann, T. Merghoub, J. D. Wolchok, S. A. Shukla, C. J. Wu, K. S. Peggs, T. A. Chan, S. R. Hadrup, S. A. Quezada, C. Swanton, Clonal neoantigens elicit T cell immunoreactivity and sensitivity to immune checkpoint blockade. *Science* **351**, 1463–1469 (2016).
11. I. A. McNeish, Neoantigens in ovarian cancer: Embarrassment of riches or needles in a haystack? *Clin. Cancer Res.* **24**, 5493–5495 (2018).
12. L. Lybaert, K. Thielemans, S. A. Feldman, S. H. van der Burg, C. Bogaert, P. A. Ott, Neoantigen-directed therapeutics in the clinic: Where are we? *Trends Cancer* **9**, 503–519 (2023).
13. H. Schuster, J. K. Peper, H. C. Bosmuller, K. Rohle, L. Backert, T. Bilich, B. Ney, M. W. Loffler, D. J. Kowalewski, N. Trautwein, A. Rabsteyn, T. Engler, S. Braun, S. P. Haen, J. S. Walz, B. Schmid-Horch, S. Y. Brucker, D. Wallwiener, O. Kohlbacher, F. Fend, H. G. Rammensee, S. Stevanovic, A. Staebler, P. Wagner, The immunopeptidomic landscape of ovarian carcinomas. *Proc. Natl. Acad. Sci. U.S.A.* **114**, E9942–E9951 (2017).
14. C. M. Laumont, T. Daouda, J. P. Laverdure, E. Bonneil, O. Caron-Lizotte, M. P. Hardy, D. P. Granados, C. Durette, S. Lemieux, P. Thibault, C. Perreault, Global proteogenomic analysis of human MHC class I-associated peptides derived from non-canonical reading frames. *Nat. Commun.* **7**, 10238 (2016).
15. C. M. Laumont, K. Vincent, L. Hesnard, E. Audemard, E. Bonneil, J. P. Laverdure, P. Gendron, M. Courcelles, M. P. Hardy, C. Cote, C. Durette, C. St-Pierre, M. Benhammadi, J. Lanoix, S. Vobecky, E. Haddad, S. Lemieux, P. Thibault, C. Perreault, Noncoding regions are the main source of targetable tumor-specific antigens. *Sci. Transl. Med.* **10**, eaau5516 (2018).

16. Q. Zhao, J.-P. Laverdure, J. Lanoix, C. Durette, C. Coté, E. Bonneil, C. M. Laumont, P. Gendron, K. Vincent, M. Courcelles, S. Lemieux, D. G. Millar, P. S. Ohashi, P. Thibault, C. Perreault, Proteogenomics uncovers a vast repertoire of shared tumor-specific antigens in ovarian cancer. *Cancer Immunol. Res.* **8**, 544–555 (2020).
17. C. Chong, M. Muller, H. Pak, D. Harnett, F. Huber, D. Grun, M. Leleu, A. Auger, M. Arnaud, B. J. Stevenson, J. Michaux, I. Bilic, A. Hirsekorn, L. Calviello, L. Simo-Riudalbas, E. Planet, J. Lubinski, M. Bryskiewicz, M. Wiznerowicz, I. Xenarios, L. Zhang, D. Trono, A. Harari, U. Ohler, G. Coukos, M. Bassani-Sternberg, Integrated proteogenomic deep sequencing and analytics accurately identify non-canonical peptides in tumor immunopeptidomes. *Nat. Commun.* **11**, 1293 (2020).
18. M. V. Ruiz Cuevas, M. P. Hardy, J. Holly, E. Bonneil, C. Durette, M. Courcelles, J. Lanoix, C. Cote, L. M. Staudt, S. Lemieux, P. Thibault, C. Perreault, J. W. Yewdell, Most non-canonical proteins uniquely populate the proteome or immunopeptidome. *Cell Rep.* **34**, 108815 (2021).
19. K. E. Scull, K. Pandey, S. H. Ramarathinam, A. W. Purcell, Immunopeptidogenomics: Harnessing RNA-seq to illuminate the dark immunopeptidome. *Mol. Cell. Proteomics* **20**, 100143 (2021).
20. Y. A. Qi, T. K. Maity, C. M. Cultraro, V. Misra, X. Zhang, C. Ade, S. Gao, D. Milewski, K. D. Nguyen, M. H. Ebrahimabadi, K. I. Hanada, J. Khan, C. Sahinalp, J. C. Yang, U. Guha, Proteogenomic analysis unveils the HLA class I-presented immunopeptidome in melanoma and EGFR-mutant lung adenocarcinoma. *Mol. Cell. Proteomics* **20**, 100136 (2021).
21. B. Zhang, M. Bassani-Sternberg, Current perspectives on mass spectrometry-based immunopeptidomics: The computational angle to tumor antigen discovery. *J. Immunother. Cancer* **11**, e007073 (2023).
22. M. Lozano-Rabella, A. Garcia-Garijo, J. Palomero, A. Yuste-Estevanez, F. Erhard, R. Farriol-Duran, J. Martin-Liberal, M. Ochoa-de-Olza, I. Matos, J. J. Gartner, M. Ghosh, F. Canals, A. Vidal, J. M. Piulats, X. Matias-Guiu, I. Brana, E. Munoz-Couselo, E. Garralda, A. Schlosser, A. Gros, Exploring the immunogenicity of noncanonical HLA-I tumor ligands identified through proteogenomics. *Clin. Cancer Res.* **29**, 2250–2265 (2023).
23. J. Chen, A. D. Brunner, J. Z. Cogan, J. K. Nunez, A. P. Fields, B. Adamson, D. N. Itzhak, J. Y. Li, M. Mann, M. D. Leonetti, J. S. Weissman, Pervasive functional translation of noncanonical human open reading frames. *Science* **367**, 1140–1146 (2020).
24. F. Erhard, L. Dolken, B. Schilling, A. Schlosser, Identification of the cryptic HLA-I immunopeptidome. *Cancer Immunol. Res.* **8**, 1018–1026 (2020).
25. T. Ouspenskaia, T. Law, K. R. Clauser, S. Klaeger, S. Sarkizova, F. Aguet, B. Li, E. Christian, B. A. Knisbacher, P. M. Le, C. R. Hartigan, H. Keshishian, A. Apffel, G. Oliveira, W. Zhang, S. Chen, Y. T. Chow, Z. Ji, I. Jungreis, S. A. Shukla, S. Justesen, P. Bachireddy, M. Kellis, G. Getz, N. Hacohen, D. B. Keskin, S. A. Carr, C. J. Wu, A. Regev, Unannotated proteins expand the MHC-I-restricted immunopeptidome in cancer. *Nat. Biotechnol.* **40**, 209–217 (2022).
26. M. S. Kim, S. M. Pinto, D. Getnet, R. S. Nirujogi, S. S. Manda, R. Chaerkady, A. K. Madugundu, D. S. Kelkar, R. Isserlin, S. Jain, J. K. Thomas, B. Muthusamy, P. Leal-Rojas, P. Kumar, N. A. Sahasrabuddhe, L. Balakrishnan, J. Advani, B. George, S. Renuse, L. D. Selvan, A. H. Patil, V. Nanjappa, A. Radhakrishnan, S. Prasad, T. Subbannayya, R. Raju, M. Kumar, S. K. Sreenivasamurthy, A. Marimuthu, G. J. Sathe, S. Chavan, K. K. Datta, Y. Subbannayya, A. Sahu, S. D. Yelamanchi, S. Jayaram, P. Rajagopalan, J. Sharma, K. R. Murthy, N. Syed, R. Goel, A. A. Khan, S. Ahmad, G. Dey, K. Mudgal, A. Chatterjee, T. C. Huang, J. Zhong, X. Wu, P. G. Shaw, D. Freed, M. S. Zahari, K. K. Mukherjee, S. Shankar, A. Mahadevan, H. Lam, C. J. Mitchell, S. K. Shankar, P. Satishchandra, J. T. Schroeder, R. Sirdeshmukh, A. Maitra, S. D. Leach, C. G. Drake, M. K. Halushka, T. S. Prasad, R. H. Hruban, C. L. Kerr, G. D. Bader, C. A. Iacobuzio-Donahue, H. Gowda, A. Pandey, A draft map of the human proteome. *Nature* **509**, 575–581 (2014).
27. R. Xiang, L. Ma, M. Yang, Z. Zheng, X. Chen, F. Jia, F. Xie, Y. Zhou, F. Li, K. Wu, Y. Zhu, Increased expression of peptides from non-coding genes in cancer proteomics datasets suggests potential tumor neoantigens. *Commun. Biol.* **4**, 496 (2021).
28. X. Yi, Y. Liao, B. Wen, K. Li, Y. Dou, S. R. Savage, B. Zhang, caAtlas: An immunopeptidome atlas of human cancer. *iScience* **24**, 103107 (2021).
29. J. R. Prensner, J. G. Abelin, L. W. Kok, K. R. Clauser, J. M. Mudge, J. Ruiz-Orera, M. Bassani-Sternberg, E. W. Deutsch, S. van Heesch, What can Ribo-seq and proteomics tell us about the non-canonical proteome? bioRxiv 541049 [Preprint] (2023). https://doi.org/10.1101/2023.05.16.541049.
30. A. Marcu, L. Bichmann, L. Kuchenbecker, D. J. Kowalewski, L. K. Freudenmann, L. Backert, L. Mühlenbruch, A. Szolek, M. Lübke, P. Wagner, T. Engler, S. Matovina, J. Wang, M. Hauri-Hohl, R. Martin, K. Kapolou, J. S. Walz, J. Velz, H. Moch, L. Regli, M. Silginer, M. Weller, M. W. Löffler, F. Erhard, A. Schlosser, O. Kohlbacher, S. Stevanović, H.-G. Rammensee, M. C. Neidert, HLA ligand Atlas: A benign reference of HLA-presented peptides to improve T-cell-based cancer immunotherapy. *J. ImmunoThe. Cancer* **9**, e002071 (2021).
31. A. M. Patch, E. L. Christie, D. Etemadmoghadam, D. W. Garsed, J. George, S. Fereday, K. Nones, P. Cowin, K. Alsop, P. J. Bailey, K. S. Kassahn, F. Newell, M. C. Quinn, S. Kazakoff, K. Quek, C. Wilhelm-Benartzi, E. Curry, H. S. Leong, Australian Ovarian Cancer Study, A. Hamilton, L. Mileshkin, G. Au-Yeung, C. Kennedy, J. Hung, Y. E. Chiew, P. Harnett, M. Friedlander, M. Quinn, J. Pyman, S. Cordner, P. O'Brien, J. Leditschke, G. Young, K. Strachan, P. Waring, W. Azar, C. Mitchell, N. Traficante, J. Hendley, H. Thorne, M. Shackleton, D. K. Miller, G. M. Arnau, R. W. Tothill, T. P. Holloway, T. Semple, I. Harliwong, C. Nourse, E. Nourbakhsh, S. Manning, S. Idrisoglu, T. J. Bruxner, A. N. Christ, B. Poudel, O. Holmes, M. Anderson, C. Leonard, A. Lonie, N. Hall, S. Wood, D. F. Taylor, Q. Xu, J. L. Fink, N. Waddell, R. Drapkin, E. Stronach, H. Gabra, R. Brown, A. Jewell, S. H. Nagaraj, E. Markham, P. J. Wilson, J. Ellul, O. McNally, M. A. Doyle, R. Vedururu, C. Stewart, E. Lengyel, J. V. Pearson, N. Waddell, A. deFazio, S. M. Grimmond, D. D. Bowtell, Whole-genome characterization of chemoresistant ovarian cancer. *Nature* **521**, 489–494 (2015).
32. C. C. Smith, S. R. Selitsky, S. Chai, P. M. Armistead, B. G. Vincent, J. S. Serody, Alternative tumour-specific antigens. *Nat. Rev. Cancer* **19**, 465–478 (2019).
33. L. Frankiw, D. Baltimore, G. Li, Alternative mRNA splicing in cancer immunotherapy. *Nat. Rev. Immunol.* **19**, 675–687 (2019).
34. C. M. Laumont, C. Perreault, Exploiting non-canonical translation to identify new targets for T cell-based cancer immunotherapy. *Cell Mol. Life Sci.* **75**, 607–621 (2018).
35. M. W. Loffler, C. Mohr, L. Bichmann, L. K. Freudenmann, M. Walzer, C. M. Schroeder, N. Trautwein, F. J. Hilke, R. S. Zinser, L. Muhlenbruch, D. J. Kowalewski, H. Schuster, M. Sturm, J. Matthes, O. Riess, S. Czemmel, S. Nahnsen, I. Konigsrainer, K. Thiel, S. Nadalin, S. Beckert, H. Bosmuller, F. Fend, A. Velic, B. Macek, S. P. Haen, L. Buonaguro, O. Kohlbacher, S. Stevanovic, A. Konigsrainer, HEPAVAC Consortium, H. G. Rammensee, Multi-omics discovery of exome-derived neoantigens in hepatocellular carcinoma. *Genome Med.* **11**, 28 (2019).
36. A. Newey, B. Griffiths, J. Michaux, H. S. Pak, B. J. Stevenson, A. Woolston, M. Semiannikova, G. Spain, L. J. Barber, N. Matthews, S. Rao, D. Watkins, I. Chau, G. Coukos, J. Racle, D. Gfeller, N. Starling, D. Cunningham, M. Bassani-Sternberg, M. Gerlinger, Immunopeptidomics of colorectal cancer organoids reveals a sparse HLA class I neoantigen landscape and no increase in neoantigens with interferon or MEK-inhibitor treatment. *J. Immunother. Cancer* **7**, 309 (2019).
37. K. Dhatchinamoorthy, J. D. Colbert, K. L. Rock, Cancer immune evasion through loss of MHC class I antigen presentation. *Front. Immunol.* **12**, 636568 (2021).
38. I. Vazquez-Garcia, F. Uhlitz, N. Ceglia, J. L. P. Lim, M. Wu, N. Mohibullah, J. Niyazov, A. E. B. Ruiz, K. M. Boehm, V. Bojilova, C. J. Fong, T. Funnell, D. Grewal, E. Havasov, S. Leung, A. Pasha, D. M. Patel, M. Pourmaleki, N. Rusk, H. Shi, R. Vanguri, M. J. Williams, A. W. Zhang, V. Broach, D. S. Chi, A. D. C. Paula, G. J. Gardner, S. H. Kim, M. Lennon, K. L. Roche, Y. Sonoda, O. Zivanovic, R. Kundra, A. Viale, F. N. Derakhshan, L. Geneslaw, S. I. Bhaloo, A. Maroldi, R. Nunez, F. Pareja, A. Stylianou, M. Vahdatinia, Y. Bykov, R. N. Grisham, Y. L. Liu, Y. Lakhman, I. Nikolovski, D. Kelly, J. Gao, A. Schietinger, T. J. Hollmann, S. F. Bakhoum, R. A. Soslow, L. H. Ellenson, N. R. Abu-Rustum, C. Aghajanian, C. F. Friedman, A. McPherson, B. Weigelt, D. Zamarin, S. P. Shah, Ovarian cancer mutational processes drive site-specific immune evasion. *Nature* **612**, 778–786 (2022).
39. M. Zhang, J. Fritsche, J. Roszik, L. J. Williams, X. Peng, Y. Chiu, C. C. Tsou, F. Hoffgaard, V. Goldfinger, O. Schoor, A. Talukder, M. A. Forget, C. Haymaker, C. Bernatchez, L. Han, Y. H. Tsang, K. Kong, X. Xu, K. L. Scott, H. Singh-Jasuja, G. Lizee, H. Liang, T. Weinschenk, G. B. Mills, P. Hwu, RNA editing derived epitopes function as cancer antigens to elicit immune responses. *Nat. Commun.* **9**, 3919 (2018).
40. L. Hesnard, C. Theriault, M. Cahuzac, C. Durette, K. Vincent, M. P. Hardy, J. Lanoix, G. O. Lavallee, J. Humeau, P. Thibault, C. Perreault, Immunogenicity of non-mutated ovarian cancer-specific antigens. *Curr. Oncol.* **31**, 3099–3121 (2024).
41. M. Harndahl, M. Rasmussen, G. Roder, I. Dalgaard Pedersen, M. Sørensen, M. Nielsen, S. Buus, Peptide-MHC class I stability is a better predictor than peptide affinity of CTL immunogenicity. *Eur. J. Immunol.* **42**, 1405–1416 (2012).
42. A. Sette, A. Vitiello, B. Reherman, P. Fowler, R. Nayersina, W. M. Kast, C. J. Melief, C. Oseroff, L. Yuan, J. Ruppert, J. Sidney, M. F. del Guercio, S. Southwood, R. T. Kubo, R. W. Chesnut, H. M. Grey, F. V. Chisari, The relationship between class I binding affinity and immunogenicity of potential cytotoxic T cell epitopes. *J. Immunol.* **153**, 5586–5592 (1994).
43. V. Jurtz, S. Paul, M. Andreatta, P. Marcatili, B. Peters, M. Nielsen, NetMHCpan-4.0: Improved peptide-MHC class I interaction predictions integrating eluted ligand and peptide binding affinity data. *J. Immunol.* **199**, 3360–3368 (2017).
44. R. Cibotti, J. M. Kanellopoulos, J. P. Cabaniols, O. Halle-Panenko, K. Kosmatopoulos, E. Sercarz, P. Kourilsky, Tolerance to a self-protein involves its immunodominant but does not involve its subdominant determinants. *Proc. Natl. Acad. Sci. U.S.A.* **89**, 416–420 (1992).
45. D. A. Gross, S. Graff-Dubois, P. Opolon, S. Cornet, P. Alves, A. Bennaceur-Griscelli, O. Faure, P. Guillaume, H. Firat, S. Chouaib, F. A. Lemonnier, J. Davoust, I. Miconnet, R. H. Vonderheide, K. Kosmatopoulos, High vaccination efficiency of low-affinity epitopes in antitumor immunotherapy. *J. Clin. Invest.* **113**, 425–433 (2004).
46. J. Menez-Jamet, C. Gallou, A. Rougeot, K. Kosmatopoulos, Optimized tumor cryptic peptides: The basis for universal neo-antigen-like tumor vaccines. *Ann. Transl. Med.* **4**, 266 (2016).

47. J. G. Abelin, D. B. Keskin, S. Sarkizova, C. R. Hartigan, W. Zhang, J. Sidney, J. Stevens, W. Lane, G. L. Zhang, T. M. Eisenhaure, K. R. Clauser, N. Hacohen, M. S. Rooney, S. A. Carr, C. J. Wu, Mass spectrometry profiling of HLA-associated peptidomes in mono-allelic cells enables more accurate epitope prediction. *Immunity* **46**, 315–326 (2017).
48. E. Kina, J. P. Laverdure, C. Durette, J. Lanoix, M. Courcelles, Q. Zhao, A. Apavaloaei, J. D. Larouche, M. P. Hardy, K. Vincent, P. Gendron, L. Hesnard, C. Theriault, M. V. Ruiz Cuevas, G. Ehx, P. Thibault, C. Perreault, Breast cancer immunopeptidomes contain numerous shared tumor antigens. *J. Clin. Invest.* **134**, e166740 (2024).
49. P. A. Ott, Z. Hu, D. B. Keskin, S. A. Shukla, J. Sun, D. J. Bozym, W. Zhang, A. Luoma, A. Giobbie-Hurder, L. Peter, C. Chen, O. Olive, T. A. Carter, S. Li, D. J. Lieb, T. Eisenhaure, E. Gjini, J. Stevens, W. J. Lane, I. Javeri, K. Nellaiappan, A. M. Salazar, H. Daley, M. Seaman, E. I. Buchbinder, C. H. Yoon, M. Harden, N. Lennon, S. Gabriel, S. J. Rodig, D. H. Barouch, J. C. Aster, G. Getz, K. Wucherpfennig, D. Neuberg, J. Ritz, E. S. Lander, E. F. Fritsch, N. Hacohen, C. J. Wu, An immunogenic personal neoantigen vaccine for patients with melanoma. *Nature* **547**, 217–221 (2017).
50. U. Sahin, E. Derhovanessian, M. Miller, B. P. Kloke, P. Simon, M. Lower, V. Bukur, A. D. Tadmor, U. Luxemburger, B. Schrors, T. Omokoko, M. Vormehr, C. Albrecht, A. Paruzynski, A. N. Kuhn, J. Buck, S. Heesch, K. H. Schreeb, F. Muller, I. Ortseifer, I. Vogler, E. Godehardt, S. Attig, R. Rae, A. Breitkreuz, C. Tolliver, M. Suchan, G. Martic, A. Hohberger, P. Sorn, J. Diekmann, J. Ciesla, O. Waksmann, A. K. Bruck, M. Witt, M. Zillgen, A. Rothermel, B. Kasemann, D. Langer, S. Bolte, M. Diken, S. Kreiter, R. Nemecek, C. Gebhardt, S. Grabbe, C. Holler, J. Utikal, C. Huber, C. Loquai, O. Tureci, Personalized RNA mutanome vaccines mobilize poly-specific therapeutic immunity against cancer. *Nature* **547**, 222–226 (2017).
51. J. S. Weber, M. S. Carlino, A. Khattak, T. Meniawy, G. Ansstas, M. H. Taylor, K. B. Kim, M. McKean, G. V. Long, R. J. Sullivan, M. Faries, T. T. Tran, C. L. Cowey, A. Pecora, M. Shaheen, J. Segar, T. Medina, V. Atkinson, G. T. Gibney, J. J. Luke, S. Thomas, E. I. Buchbinder, J. A. Healy, M. Huang, M. Morrissey, I. Feldman, V. Sehgal, C. Robert-Tissot, P. Hou, L. Zhu, M. Brown, P. Aanur, R. S. Meehan, T. Zaks, Individualised neoantigen therapy mRNA-4157 (V940) plus pembrolizumab versus pembrolizumab monotherapy in resected melanoma (KEYNOTE-942): A randomised, phase 2b study. *Lancet* **403**, 632–644 (2024).
52. Y. Kong, C. M. Rose, A. A. Cass, A. G. Williams, M. Darwish, S. Lianoglou, P. M. Haverty, A. J. Tong, C. Blanchette, M. L. Albert, I. Mellman, R. Bourgon, J. Greally, S. Jhunjhunwala, H. Chen-Harris, Transposable element expression in tumors is associated with immune infiltration and increased antigenicity. *Nat. Commun.* **10**, 5228 (2019).
53. B. Shraibman, D. M. Kadosh, E. Barnea, A. Admon, Human Leukocyte Antigen (HLA) peptides derived from tumor antigens induced by inhibition of DNA methylation for development of drug-facilitated immunotherapy. *Mol. Cell. Proteomics* **15**, 3058–3070 (2016).
54. J. Attig, G. R. Young, L. Hosie, D. Perkins, V. Encheva-Yokoya, J. P. Stoye, A. P. Snijders, N. Ternette, G. Kassiotis, LTR retroelement expansion of the human cancer transcriptome and immunopeptidome revealed by de novo transcript assembly. *Genome Res.* **29**, 1578–1590 (2019).
55. K. K. Mangalaparthi, A. K. Madugundu, Z. C. Ryan, K. Garapati, J. A. Peterson, G. Dey, A. Prakash, A. Pandey, Digging deeper into the immunopeptidome: Characterization of post-translationally modified peptides presented by MHC I. *J. Proteins Proteom.* **12**, 151–160 (2021).
56. M. Bassani-Sternberg, Mass spectrometry based immunopeptidomics for the discovery of cancer neoantigens. *Methods Mol. Biol.* **1719**, 209–221 (2018).
57. A. Dobin, C. A. Davis, F. Schlesinger, J. Drenkow, C. Zaleski, S. Jha, P. Batut, M. Chaisson, T. R. Gingeras, STAR: Ultrafast universal RNA-seq aligner. *Bioinformatics* **29**, 15–21 (2013).
58. M. Pertea, G. M. Pertea, C. M. Antonescu, T. C. Chang, J. T. Mendell, S. L. Salzberg, StringTie enables improved reconstruction of a transcriptome from RNA-seq reads. *Nat. Biotechnol.* **33**, 290–295 (2015).
59. J. Fritsche, B. Rakitsch, F. Hoffgaard, M. Romer, H. Schuster, D. J. Kowalewski, M. Priemer, V. Stos-Zweifel, H. Horzer, A. Satelli, A. Sonntag, V. Goldfinger, C. Song, A. Mahr, M. Ott, O. Schoor, T. Weinschenk, Translating immunopeptidomics to immunotherapy-decision-making for patient and personalized target selection. *Proteomics* **18**, e1700284 (2018).
60. A. T. Kong, F. V. Leprevost, D. M. Avtonomov, D. Mellacheruvu, A. I. Nesvizhskii, MSFragger: Ultrafast and comprehensive peptide identification in mass spectrometry-based proteomics. *Nat. Methods* **14**, 513–520 (2017).
61. D. P. Granados, D. Sriranganadane, T. Daouda, A. Zieger, C. M. Laumont, O. Caron-Lizotte, G. Boucher, M. P. Hardy, P. Gendron, C. Cote, S. Lemieux, P. Thibault, C. Perreault, Impact of genomic polymorphisms on the repertoire of human MHC class I-associated peptides. *Nat. Commun.* **5**, 3600 (2014).
62. S. Kaabinejadian, C. Barra, B. Alvarez, H. Yari, W. H. Hildebrand, M. Nielsen, Accurate MHC motif deconvolution of immunopeptidomics data reveals a significant contribution of DRB3, 4 and 5 to the total DR immunopeptidome. *Front. Immunol.* **13**, 835454 (2022).
63. N. Rapin, I. Hoof, O. Lund, M. Nielsen, MHC motif viewer. *Immunogenetics* **60**, 759–765 (2008).
64. B. Reynisson, B. Alvarez, S. Paul, B. Peters, M. Nielsen, NetMHCpan-4.1 and NetMHCIIpan-4.0: Improved predictions of MHC antigen presentation by concurrent motif deconvolution and integration of MS MHC eluted ligand data. *Nucleic Acids Res.* **48**, W449–W454 (2020).
65. A. R. Ghazi, K. Sucipto, A. Rahnavard, E. A. Franzosa, L. J. McIver, J. Lloyd-Price, E. Schwager, G. Weingart, Y. S. Moon, X. C. Morgan, L. Waldron, C. Huttenhower, High-sensitivity pattern discovery in large, paired multiomic datasets. *Bioinformatics* **38**, i378–i385 (2022).
66. T. Vardam-Kaur, L. B. Pathangey, D. J. McCormick, P. L. Bergsagel, P. A. Cohen, S. J. Gendler, Multipeptide stimulated PBMCs generate T(EM)/T(CM) for adoptive cell therapy in multiple myeloma. *Oncotarget* **12**, 2051–2067 (2021).
67. M. Wolfl, P. D. Greenberg, Antigen-specific activation and cytokine-facilitated expansion of naive, human $CD8^+$ T cells. *Nat. Protoc.* **9**, 950–966 (2014).
68. G. Dolton, K. Tungatt, A. Lloyd, V. Bianchi, S. M. Theaker, A. Trimby, C. J. Holland, M. Donia, A. J. Godkin, D. K. Cole, P. T. Straten, M. Peakman, I. M. Svane, A. K. Sewell, More tricks with tetramers: A practical guide to staining T cells with peptide-MHC multimers. *Immunology* **146**, 11–22 (2015).

Acknowledgments: We would like to thank P. Sen for efforts in preparing mirror plots for MS/MS spectra. We thank the Mayo Clinic Arizona Flow Cytometry Core for supporting this study. **Funding:** This study was supported by the High-Definition Therapeutics Grant Award (M.C.) from the Mayo Clinic Center for Individualized Medicine. Work in this publication was supported by the Mayo Clinic Comprehensive Cancer Center Grant Support Grant (P30 CA015083) from the National Cancer Institute (NCI). This work was supported in part by a pilot grant from NCI's CPTAC program to M.C. and A.P. (U01CA271410). **Author contributions:** Conceptualization: M.C. and R.R.; methodology: R.R., K.K.M., and L.P.; investigation: R.R. and K.K.M.; software: A.K.M. and E.J.; formal analysis: R.R., K.K.M., E.J., E.C., and A.K.M.; resources: K.B. and P.M.; visualization: R.R., K.K.M., and E.J.; supervision: M.C. and A.P.; writing—original draft: R.R., K.K.M., E.J., and M.C.; writing—review and editing: A.P., M.C., R.R., K.B., E.J., A.K.M., and P.M.; project administration: M.C. and A.P.; funding acquisition: M.C. All authors have read and agreed to the published version of the manuscript. **Competing interests:** The authors declare that they have no competing interests. **Data and materials availability:** The MS proteomic data have been deposited to the ProteomeXchange Consortium (http://proteomecentral.proteomexchange.org/cgi/GetDataset) via the PRIDE partner repository with the dataset identifier PXD055609. BAM files of paired-end RNA-seq data are available through National Center for Biotechnology Information Sequence Read Archive (SRA) project PRJNA1160863. For evaluating cryptic antigen expression across various stages of OC, dataset deposited under accession number EGAD00001000877 in European Genome-Phenome Archive was used. All other data needed to evaluate the conclusions in the paper are present in the paper and/or the Supplementary Materials.

Submitted 16 September 2024
Accepted 16 January 2025
Published 19 February 2025
10.1126/sciadv.ads7405